Available online at www.sciencedirect.com
SCIENCE DIRECT®
International Journal of Heat and Fluid Flow 24 (2003) 14–22
International Journal of HEAT AND FLUID FLOW
www.elsevier.com/locate/ijhff

Transient heat transfer measurements using thermochromic liquid crystal. Part 1: An improved technique

Paul J. Newton, Youyou Yan [1], Nia E. Stevens [2], Simon T. Evatt [3], Gary D. Lock, J. Michael Owen *

Department of Mechanical Engineering, University of Bath, Bath BA2 7AY, UK

Received 28 January 2002; accepted 4 August 2002

Abstract

It is common practice to employ thermochromic liquid crystal (TLC) to determine heat transfer coefficients, h, in transient experiments. The method relies on the solution of Fourier's conduction equation, usually with the boundary condition of a step-change in air temperature. In practice a step-change can be difficult to achieve, and a more general solution to the one-dimensional conduction equation is presented here for a "slow transient," where the rise in air temperature is represented by an exponential series. An experimental method, based on this technique, requires only a single measurement of surface temperature history, and this has the advantage that narrow-band TLC can be used. As an example, measurements of h are presented from an experiment modelling the internal flow of cooling air inside a gas turbine engine. The measurements are analysed using both the conventional step-change method and the exponential-series technique, and the results show that using the step-change method can give rise to significant errors in the calculated values of h. The new technique should be applicable to many other slow transient heat transfer measurements.

Keywords: Thermochromic liquid crystal; Transient heat transfer

1. Introduction

Thermochromic liquid crystal (TLC) is now used widely to measure surface temperature. In a transient experiment, if the time at which the TLC changes colour is known (so that the surface temperature is also known) then the heat transfer coefficient, h, can be calculated from the one-dimensional solution of Fourier's conduction equation for a semi-infinite wall. The use of TLC to determine h in this way has been reported broadly, and the reader is referred to Jones and Hippensteele (1988), Kasagi et al. (1989), Camci et al. (1991) and Baughn (1995).

In most transient experiments, a *step-change* in the air temperature is created. (Although "air" is used throughout this paper, the principles apply to all fluids.) Knowing the surface temperature of the heated wall, T_w, at time t, h can be found from a relatively simple analytical solution of Fourier's equation (see Section 2). For this case, narrow-band TLC (with a "transition temperature" range of around 1 °C) is commonly used. The uncertainty in the surface temperature is relatively small (of the order of 0.1 °C), and by judicious choice of the TLC the uncertainty in h can also be small (see Yan and Owen, 2002).

In some experiments it is not possible to create a step-change in the air temperature: as a result of thermal inertia in the heater, or in the ducting upstream of the test section, the air takes time to reach its steady-state temperature. Such cases, which the authors have experienced in their own experiments, are referred to here as *slow transients*. Wide-band TLC (with a transition-temperature range of, say, 20 °C) can be used to measure the variation of surface temperature with time, and, by

* Corresponding author. Tel.: +44-01225-386115; fax: +44-01225-386928.
E-mail address: j.m.owen@bath.ac.uk (J.M. Owen).
[1] Present address: City University, London, UK.
[2] Present address: Imperial College of Science, Technology and Medicine, London, UK.
[3] Present address: Accenture plc, London, UK.

0142-727X/02/$ - see front matter © 2002 Elsevier Science Inc. All rights reserved.
PII: S0142-727X(02)00206-0

Nomenclature

b	radial location of pre-swirl nozzles
c	specific heat of wall
c_j	weighting terms in series solution
C_p	specific heat at constant pressure of air
f(β)	step-change solution of Fourier's equation
F	time-invariant adiabatic-wall parameter ($T_{aw} - T_a$)
g	exponential solution of Fourier's equation ($g(\beta, \beta_\tau), g(\beta, \lambda_j)$)
h	heat transfer coefficient ($q_w/(T_{aw} - T_w)$)
k	thermal conductivity of wall
m	number of terms in exponential series
N	number of data in sample
P	uncertainty in measured value (95% confidence estimate)
q_w	heat flux from air to wall
r	radius from axis of rotation
R	recovery factor
S	standard deviation
t	time
$T(x,t)$	temperature inside wall
$T_a(t)$	total-temperature of air
$T_{aw}(t)$	adiabatic-wall temperature
$T_w(t)$	surface temperature of wall
U	free-stream velocity
V_ϕ	tangential component of velocity
x	normal distance from surface towards interior of wall
α	thermal diffusivity of wall (k/ρc)
β	parameter in step-change solution ($h\sqrt{t/\rho ck}$)
β_τ	parameter in exponential solution ($h\sqrt{\tau/\rho ck}$)
ΔT_a	difference between fitted and measured values of T_a
Γ	component of amplification parameter
κ	thermal property of wall (ρck)
λ	non-dimensional time parameter ($\sqrt{t/\tau}$)
θ_{aw}	adiabatic temperature difference ($T_{aw} - T_o$)
θ_w	temperature difference ($T_w - T_o$)
Θ	non-dimensional temperature ($(T_w - T_o)/(T_{aw,\infty} - T_o)$)
ρ	density of wall
$\phi(\lambda)$	function of λ in exponential solution of Fourier's equation
Φ_h	amplification parameter for uncertainty in h
Ω	angular speed of rotating disc
τ	time constant

Subscripts

c	value in fluid core outside boundary layers
h	with reference to h
j	jth term of exponential series
min	minimum value
o	value at $t = 0$
t	with reference to time
T	with reference to maximum value of P_{T_w}, P_{T_o} and $P_{T_{aw}}$
T_{aw}	with reference to adiabatic-wall temperature
T_o	with reference to initial temperature
T_w	with reference to surface temperature
β	with reference to β
Θ	with reference to Θ
∞	value as $t \to \infty$

Superscript

$*$	Value for special case where uncertainties in measured temperatures are equal to each other

the use of Duhamel's method, Fourier's equation can be solved and h determined. Unfortunately, the uncertainty in the measurement of surface temperature using wide-band TLC is an order-of-magnitude greater than that using narrow-band, and this results in a relatively large uncertainty in h.

Ireland and Jones (2000) summarise solutions of Fourier's equation for fluid temperatures modelled by different analytical functions. In addition to the step-change and Duhamel models mentioned above, solutions are also provided for a "ramp" of constant slope as well as a series of ramps. These authors found that ramps were appropriate when the air temperature decreased with time, as occurs when batteries are used to provide the electrical power for the heater.

For the special case where the air temperature rises exponentially with time, Gillespie et al. (1998) obtained an analytical solution of Fourier's equation, and their solution forms an important building block for the method described here. In many experiments, the variation of air temperature with time cannot be accurately described by a simple exponential fit, but it may be approximated with good accuracy by an exponential series. This leads to an analytical solution of Fourier's equation, from which h can be readily determined. The advantage of the "exponential-series technique" is that, just as for the step-change case, a single narrow-band crystal can be used to determine h. This allows the accuracy of the simple step-change method to be brought to the more difficult case of the slow transient.

Before proceeding with the analysis, it is useful to define the convective heat transfer coefficient as follows:

$$q_w = h(T_{aw} - T_w) \tag{1.1}$$

where q_w is the surface heat flux from the air to the wall, T_w the surface temperature of the wall, and T_{aw} the adiabatic-wall temperature. T_{aw} is related to the total-temperature of the air, T_a, and the difference between these two temperatures depends on the fluid dynamics. For example, for boundary-layer flow over a flat plate with a free-stream velocity U,

$$T_{aw} = T_a - (1 - R)\frac{U^2}{2c_p} \tag{1.2}$$

where R is the recovery factor.

It is assumed here that the relationship between T_{aw} and T_a is invariant with time and is known in advance of the experiment. If T_{aw} is unknown then, in principle, both h and T_{aw} can be determined using two narrow-band crystals. However, as shown by Yan and Owen (2002), the resulting uncertainty in h will be larger than for the single-crystal case, and great care is needed to select suitable crystals to minimise the uncertainties in h and T_{aw}.

It is also assumed that h is invariant with time. This will not be true when buoyancy effects are significant such that h varies with the temperature level. Also it may not be true in some forced convection cases where h depends on the distribution of surface temperature (see, for example, Butler and Baughn, 1996). For such cases, tests with more than one crystal could be used to determine the sensitivity of h to the level or distribution of surface temperature.

The solution of Fourier's equation for a slow transient is presented in Section 2. In Section 3, the apparatus used to generate the experimental data is outlined. Section 4 describes how the parameters of the exponential series are calculated, and Section 5 gives examples of the applications of the method to measured data. A summary of the conclusions is presented in Section 6.

Part 2 of this paper (Owen et al., 2003) is concerned with the effect of uncertainties in the measured temperatures on the uncertainty in the calculated value of h. For brevity, Part 2 is referred to below as 2.

2. Solution of Fouriers equation for a slow transient

The one-dimensional Fourier equation for a semi-infinite wall, with a temperature $T = T(x,t)$, can be written as

$$\frac{\partial T}{\partial t} = \alpha\frac{\partial^2 T}{\partial x^2} \tag{2.1}$$

For the case considered here, the initial condition is

$$t = 0 : T(x,0) = T_o \tag{2.2}$$

and the convective boundary condition is

$$x = 0 : -k\left(\frac{\partial T}{\partial x}\right) = h(T_{aw} - T_w) \tag{2.3}$$

where $T_w = T_w(t)$ is the surface temperature of the wall and $T_{aw} = T_{aw}(t)$ is the adiabatic-wall temperature at time t. It should be noted that, at $t = 0$, $T_o = T_{aw,o}$. The semi-infinite-wall assumption is that $T(x,t) = T_o$ as $x \to \infty$.

It is convenient to express the adiabatic-wall temperature as

$$T_{aw}(t) - T_a(t) = F \tag{2.4}$$

where T_a is the total-temperature of the air at time t and F is invariant with time. Note that for the flat-plate example considered in Section 1, $F = (R-1)U^2/2c_p$. It follows from Eq. (2.4) that, at $t = 0$, $T_o = T_{aw,o} = T_{a,o} + F$.

2.1. Step-change case

One well-known solution to Eq. (2.1) is the case of a step-change in air temperature from $T_a = T_{a,o}$ at $t = 0$ to $T_a = T_{a,\infty}$ for $t > 0$. For this case, the solution (see, for example, Schultz and Jones, 1973) is

$$\Theta = \frac{T_w - T_o}{T_{aw,\infty} - T_o} = f(\beta) \tag{2.5}$$

where

$$f(\beta) = 1 - e^{\beta^2}\operatorname{erfc}(\beta), \tag{2.6}$$

$$\beta = \frac{h\sqrt{t}}{\sqrt{\rho c k}} \tag{2.7}$$

and

$$T_{aw,\infty} = T_{a,\infty} + F \tag{2.8}$$

If T_w, $T_{aw,\infty}$ and T_o are known, then β can be found from the numerical solution of Eq. (2.5). As T_w is the temperature at which the TLC changes colour, and as t is the time at which this change occurs, then h can be found from Eq. (2.7) for a substrate of known thermal properties.

2.2. Exponential case

Consider next the case where T_a increases exponentially with time from $T_a = T_{a,o}$ at $t = 0$ to $T_a = T_{a,\infty}$ as t tends to infinity, such that

$$T_a(t) = T_{a,o} + (T_{a,\infty} - T_{a,o})(1 - e^{-t/\tau}) \tag{2.9}$$

where τ is the time-constant of the exponential rise in air temperature. Using the results of Gillespie et al. (1998), the solution of Eq. (2.1) for this case can be written as

$$\Theta = \frac{T_w - T_o}{T_{aw,\infty} - T_o} = g(\beta, \beta_\tau) \tag{2.10}$$

where

$$g(\beta,\beta_\tau)=1-\frac{1}{1+\beta_\tau^2}e^{\beta^2}\operatorname{erfc}(\beta)-e^{-t/\tau}\frac{\beta_\tau^2}{1+\beta_\tau^2}\times\left\{1+\frac{1}{\beta_\tau}\left[\frac{1}{\pi}\sqrt{\frac{t}{\tau}}+\frac{2}{\pi}\sum_{n=1}^{\infty}\frac{1}{n}e^{-n^2/4}\sinh\left(n\sqrt{\frac{t}{\tau}}\right)\right]\right\} \tag{2.11}$$

and

$$\beta_\tau=\frac{h\sqrt{\tau}}{\sqrt{\rho ck}} \tag{2.12}$$

If $\tau=0$, then Eq. (2.10) reduces to (2.5).

Fig. 1 shows the effect of β_τ on the variation of β with Θ according to Eq. (2.10). Curves are shown for $0\leqslant\beta_\tau\leqslant 10$ for increments of 0.05; the curve for $\beta_\tau=0$ corresponds to $f(\beta)$, given by Eq. (2.6).

2.3. Exponential series

For the more general case, it is assumed that the rise in air temperature can be approximated by a series of m exponential functions such that

$$T_a(t)=T_{a,o}+\sum_{j=1}^{m}T_{a,j}(1-e^{-t/\tau_j}) \tag{2.13}$$

where the $T_{a,j}$ and τ_j are constant amplitudes and time constants, respectively.

The adiabatic-wall temperature is given by

$$T_{aw}(t)=T_o+\sum_{j=1}^{m}T_{a,j}(1-e^{-t/\tau_j}) \tag{2.14}$$

where $T_o=T_{aw,o}=T_{a,o}+F$. As $t\to\infty$,

$$T_{aw,\infty}=T_o+\sum_{j=1}^{m}T_{aw,j} \tag{2.15}$$

where $T_{aw,j}=T_{a,j}$.

The temperature inside the wall is

$$T(x,t)=T_o+\sum_{j=1}^{m}T_j(x,t) \tag{2.16}$$

which must satisfy Fourier's equation. This requires that, for $j=1$ to m,

$$\frac{\partial T_j}{\partial t}=\alpha\frac{\partial^2 T_j}{\partial x^2} \tag{2.17}$$

with the conditions that

$$t=0: T_j=0 \tag{2.18}$$

and

$$x=0: -k\frac{\partial T_j}{\partial x}=h(T_{aw,j}-T_{w,j}) \tag{2.19}$$

Using the result of Eq. (2.10) it follows that

$$\frac{T_{w,j}}{T_{aw,j}}=g(\beta,\beta_{\tau_j}) \tag{2.20}$$

where τ_j is used in Eq. (2.12) to give β_{τ_j}.

As

$$T_w(t)=T_o+\sum_{j=1}^{m}T_{w,j}(t) \tag{2.21}$$

the general solution for the wall temperature is

$$\Theta=\frac{T_w-T_o}{T_{aw,\infty}-T_o}=\sum_{j=1}^{m}\frac{T_{a,j}}{T_{aw,\infty}-T_o}g(\beta,\beta_{\tau_j}) \tag{2.22}$$

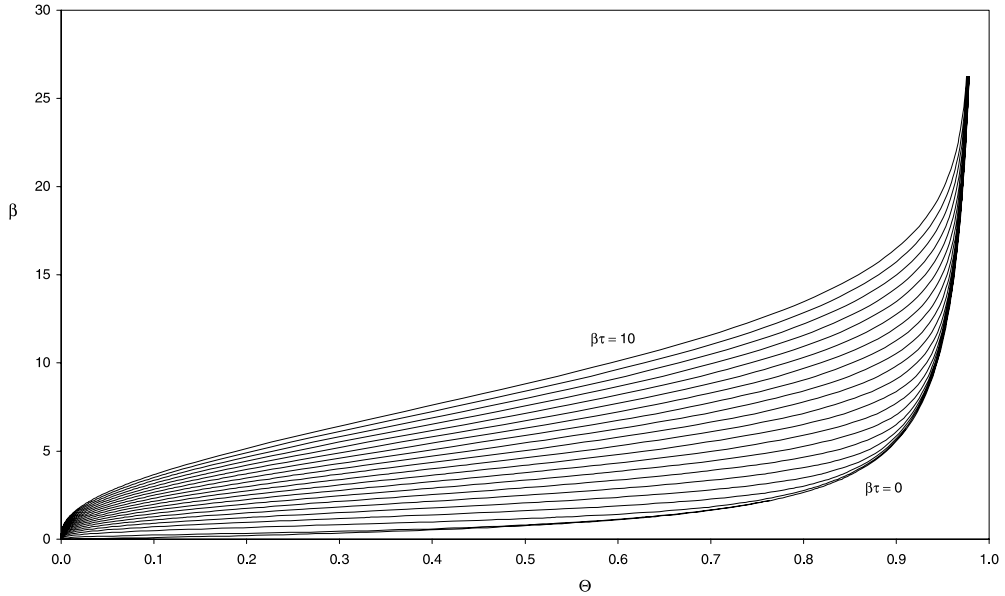

Fig. 1. Effect of β_τ on variation of β with Θ according to Eq. (2.10).

where $T_{aw,\infty}$ is given by the Eq. (2.15). For the case where $m = 1$, $T_{aw,\infty} - T_o = T_{a,1}$, and Eq. (2.22) reduces to (2.10).

Once the values of $T_{a,j}$ and τ_j have been determined from the measured air temperature, as described in Section 4, h can be found from the numerical solution of Eq. (2.22).

3. Description of experimental apparatus

The apparatus is not described in detail as the paper has been written to emphasise the experimental technique and analysis rather than the physical significance of the data collected. However, two important points should be made: (a) the new analysis became necessary due to the limitations of the apparatus, which could not provide a step-change in the air temperature at the test section; and (b) these limitations probably occur in many experimental facilities employing the transient TLC technique.

Experiments were conducted using a scaled model of a gas-turbine rotor–stator cavity featuring pre-swirled cooling air. The purpose of the study is to investigate the fluid dynamics and heat transfer associated with the motion of cooling air within this cavity. Fig. 2 is a photograph of the test section featuring, in the foreground, a transparent polycarbonate rotating disc, which permits optical access to the rotor–stator cavity and, in the background, the stationary disc representing the stator. Sectors of the rotating disc were sprayed with TLC and black paint.

The air enters the test section through the stator at low radius via nozzles (marked A in Fig. 2) which swirl the air at 20° to the tangential direction. The cooling air flows radially outward between the rotating disc and the stator, exiting through receiver holes (marked B) in the rotating disc representing the entrance to the blade-cooling passages in the engine. Details of the test section and the magnitude of the relevant non-dimensional parameters (rotational Reynolds number, non-dimensional flow rate, pre-swirl ratio) are given in Yan et al. (2002), while previous research on rotating-disc flow and heat transfer with pre-swirled cooling air is described by Pilbrow et al. (1999) and Karabay et al. (2001).

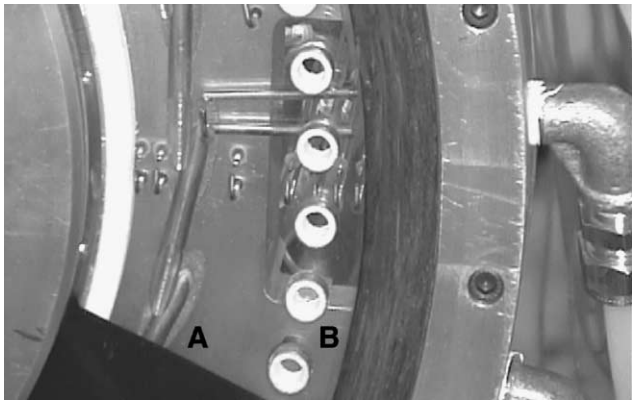

Fig. 2. Photograph of test section.

Local heat transfer coefficients on the rotating disc are determined from surface-temperature measurements using thermochromic liquid crystal. The experiments, which are transient and conducted under known thermal boundary conditions, rely on the accurate measurement of the time taken for the narrow-band TLC on the rotor surface to reach a unique value of hue, which has been calibrated against temperature. Two narrow-band crystals are used, one active at approximately 30 °C and the other at approximately 40 °C; only the results for the 40 °C crystal are discussed here. Wide-band TLC is also used in the experiments to measure the initial temperature of the disc. The crystals are sprayed on the disc in sectors which are viewed by a digital video camera, running at 25 frames per second, under the illumination of a strobe light synchronised to the disc frequency. A thin layer of black paint is used to provide contrast to the colour play of the TLC. The in situ calibration of the crystals is not discussed here, though it should be noted that the hue was measured as a function of temperature over a range of strobe frequencies corresponding to rotational disc speeds up to 5000 rpm.

A schematic diagram of the experimental apparatus is shown in Fig. 3. The primary air from the mesh-heater unit enters the rotor–stator cavity via the pre-swirl nozzles, and most (>90%) leaves through the receiver holes in the rotating disc. Some of the air is allowed to leak past the labyrinth seal at the periphery of the cavity, and this leakage flow rate is controlled by secondary-air supplied to the seal. The flow rates were measured using orifice plates designed to British Standards (BS1042). All pipework downstream of the mesh heaters is thermally insulated using low-conductivity Rhoacell, a closed-pore structural foam with low thermal conductivity (typically 0.03 W/mK at 20 °C). This pipework has three main components: a 350-mm length of rectangular cross-section, a 350-mm length of circular cross-section, and a radial diffuser; there is also a short entry length into the pre-swirl nozzles. Pitot tubes and static-pressure taps are used to measure the pressure and air velocity in the cavity.

A mesh heater, designed using the method of Ireland (Gillespie et al., 2001), is used to generate an abrupt change in the air temperature and to create a well-controlled thermal boundary condition for the transient experiment. The mesh is made of 90-μm-diameter stainless-steel wire with an open area of 38% and overall dimensions of 60 by 120 mm. The mesh is soldered to bus-bars, and the additional support of three strengthening rods of 3 mm diameter was required due to the large flow rates of air through the mesh. Typically a

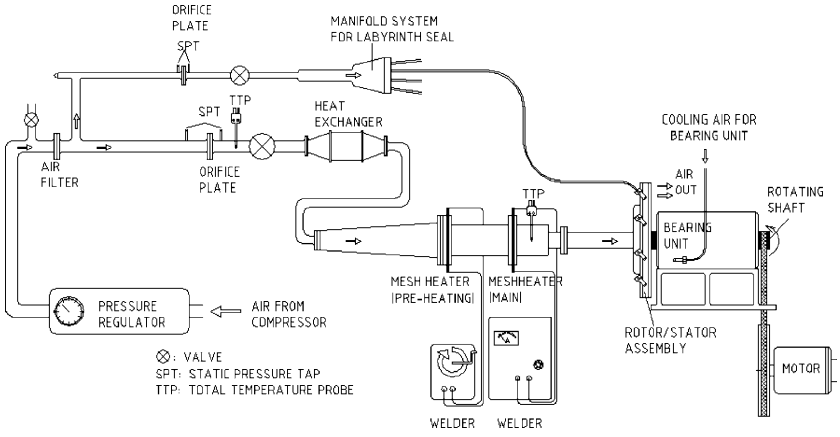

Fig. 3. Schematic diagram of experimental apparatus.

current of 150 amps is used to increase the gas temperature across the mesh heater by 40 °C for a mass flow rate of 0.1 kg/s.

Before the main mesh heater was switched on, the apparatus was left running, at the required speed and flow rate, to enable it to reach thermal equilibrium. When the air from the compressor was not equal to the ambient temperature in the laboratory, it was either cooled by a heat exchanger or heated by a second mesh heater upstream of the main heater. In practice, it was not possible to achieve perfect thermal equilibrium, and there was always a small temperature difference between the rotating disc and the air, as discussed in Section 5.

A typical example of the measured total-temperature of the cooling air is shown in Fig. 4. The data was recorded using a fast-response total-temperature probe comprising a K-type thermocouple with a 25 μm diameter wire, carefully calibrated for recovery factor. The measurements were made at two locations. The first location is immediately downstream of the mesh heater, and here the temperature is observed to exhibit a virtual step-change from an initial value of around 23 °C to a final steady-state temperature of 57 °C. The second location is at the exit of the pre-swirl nozzles, where the air enters the test section. Despite the thermal insulation in the pipes, the air temperature at this latter location is seen to rise exponentially from its initial value towards a final steady-state temperature. Typically the crystal colour-change times on the disc surface ranged between 1 and 20 s (depending on the local heat transfer coefficient), and these times are of similar magnitude to the time constants of the exponential rise in gas temperature.

In the next section it is shown that the air temperature can be accurately modelled as an exponential series of three terms. It seems likely that three time constants are required because there are three distinct geometric sections to the duct downstream of the heater mesh, as discussed above.

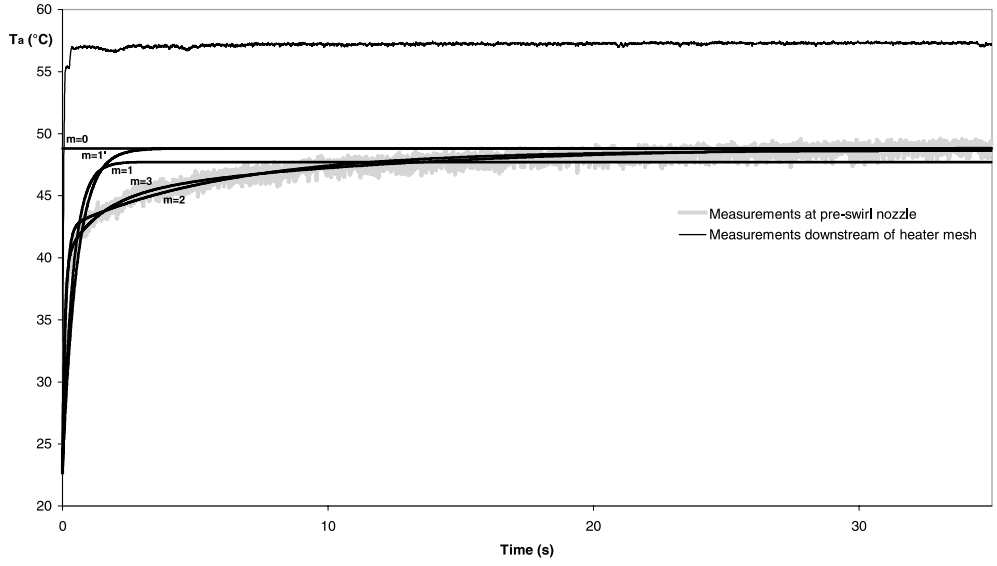

Fig. 4. Variation of T_a with time.

4. Parameters for the exponential series

The time taken for the wall to reach the temperature of the calibrated narrow-band crystal, T_w, from an initial temperature, T_o, was measured at each pixel on the active surface of the disc in the field-of-view of the digital camera. A "median filter," using the median of nine adjacent pixels, was used to reduce the uncertainty in the measured values of T_w.

The parameters for curve fits for a series with $m = 1$, 2 and 3 exponentials were determined for the air temperature in Fig. 4, and these are given in Table 1, and the curve fits are shown in Fig. 4. Two different fitting methods were employed. The curves were generated from the data using a least-squares algorithm with the starting point "anchored" at the initial temperature, $T_{a,0}$. This method yielded m values of τ_j and $T_{a,j}$ for each fit. The value of $T_{a,\infty}$ for the step-change case ($m = 0$) was based on the statistical average of the last 100 data points in the measured air temperature history.

Table 1 shows that this method determined very similar values of $T_{a,\infty}$ for the $m = 0$, 2 and 3 cases. The $m = 1$ curve significantly under-predicts $T_{a,\infty}$ relative to the others. Consequently, an alternative method was employed for the single exponential case, and this is labelled as $m = 1'$. This curve was generated using $T_{a,\infty}$ based on the statistical average of the last 100 data points in the measured air temperature history, as for the step-change case; $T_{a,0}$ was the same as for the other cases. The single exponential fit ($m = 1$) over-predicts the air temperature in the first 10 s and under-predicts the final temperature.

The greater the number of terms in the exponential series, the better the fit. The "quality of fit" is quantified by a mean difference ΔT_a between the temperature generated by the curve fit and the measured value, and by the standard deviation $S(\Delta T_a)$ of this difference. These are also shown in Table 1.

The effect of using the different curve-fits on the calculation of heat transfer coefficient is discussed below. Although the air temperature history shown here is specific to one test in one particular experimental apparatus, it is believed to be typical of distributions that occur in many other set-ups used in transient experiments with TLC.

5. Experimental results

5.1. Initial temperature

According to the theoretical steady-state results of Karabay et al. (2001) for a pre-swirl rotating-disc system, the adiabatic-wall temperature is given by

$$T_{aw} - T_c = \frac{1}{2C_p}\left\{R(\Omega r - V_{\phi,c})^2 - V_{\phi,c}^2\right\} \tag{5.1}$$

where T_c and $V_{\phi,c}$ are the total temperature and tangential component of velocity, respectively, in the core of fluid outside the boundary layers at radius r. R is the recovery factor, taken as $Pr^{1/3}$ (i.e., $R = 0.89$). As there are no total-temperature measurements in the core, it is assumed here that $T_c = T_a$, the measured temperature of the air entering the system, so that

$$T_{aw}(t) - T_a(t) = \frac{1}{2C_p}\left\{R(\Omega r - V_{\phi,c})^2 - V_{\phi,c}^2\right\} \tag{5.2}$$

The right-hand-side of Eq. (5.2) corresponds to F in Eq. (2.4).

If the disc were truly adiabatic then, at $t = 0$, its initial temperature, T_o, would be equal to the adiabatic-wall temperature, $T_{aw,o}$, where $T_{aw,o} - T_{a,o} = F$. Fig. 5 shows the variation of $T_{aw,o} - T_{a,o}$ with non-dimensional radius, r/b: the solid line refers to values deduced from the measurements of the wall temperature, T_w (made using wide-band TLC), assuming that $T_w = T_{aw,o} = T_o$; the symbols refer to the "theoretical values" determined according to Eq. (5.2) with measured values of T_a and $V_{\phi,c}$. Apart from the region near the pre-swirl nozzles ($r/b = 0.74$), most of the measured and theoretical values of $T_{aw,o}$ are within 0.5 °C.

For the calculation of the heat transfer coefficients discussed below, T_{aw} was calculated from Eq. (5.2), using fitted values of $V_{\phi,c}$; T_o was obtained from the least-squares fit of the theoretical values, which is shown in Fig. 5.

5.2. Heat transfer coefficients

Measurements of heat transfer coefficient are available at most positions on the disc surface viewed by the camera, but only data measured along a disc radius

Table 1
Statistical comparison of curve fits, $T_{a,0} = 22.7$ °C

Number of terms	$T_{a,\infty}$ (°C)	$j = 1$		$j = 2$		$j = 3$		ΔT_a (°C)	$S(\Delta T_a)$ (°C)
		$T_{a,j}$ (°C)	τ_j(s)	$\tau_{a,j}$ (°C)	τ_j(s)	$T_{a,j}$ (°C)	τ_j(s)		
$m = 0$ (step)	48.80							1.329	1.963
$m = 1$	47.72	25.04	0.394					−0.030	1.353
$m = 1'$	48.80	26.12	0.540					0.923	1.426
$m = 2$	48.65	19.64	0.123	6.32	6.14			0.008	0.451
$m = 3$	49.06	17.01	0.086	5.08	1.33	4.30	11.63	−0.003	0.391

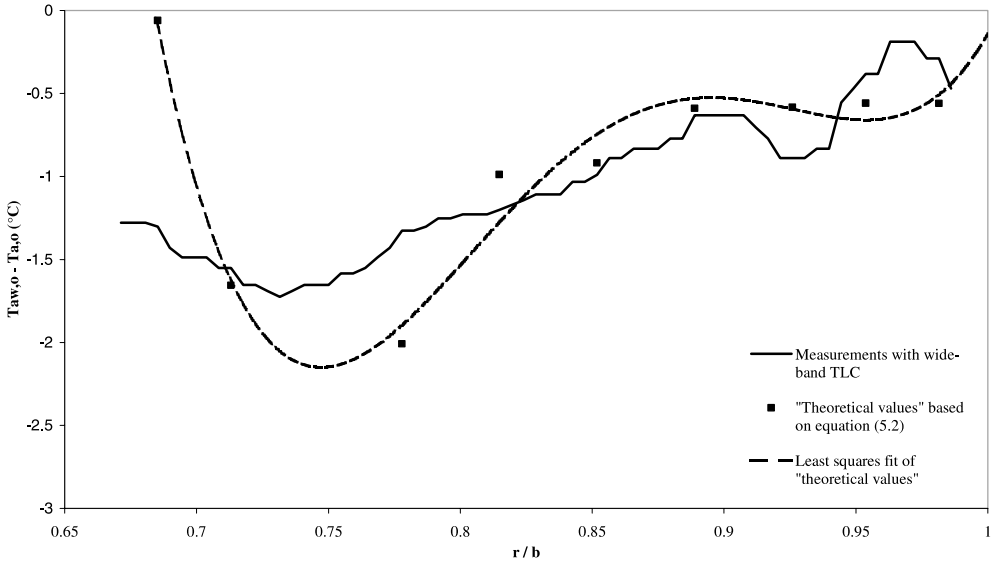

Fig. 5. Radial variation of adiabatic-wall temperature at $t = 0$.

midway between two receiver holes are presented here. Heat transfer coefficients based on measurements using the 40 °C narrow-band TLC are plotted against non-dimensional radius, r/b, in Fig. 6. The heat transfer coefficients were calculated, using the results of Section 2, for an air temperature based on the five models described in Section 4: the step-change ($m = 0$), the single exponentials ($m = 1$ and $1'$), two exponentials ($m = 2$), and three exponentials ($m = 3$).

All the data exhibit a peak opposite the pre-swirl nozzles at $r/b = 0.74$, which is associated with the impingement of the hot air on the disc surface. There is also a peak near the receiver holes at $r/b = 0.95$, associated with the three-dimensional flow exiting through the holes. Though these phenomena are of importance to the turbine designer, the interest here is in the comparison of the measurements determined by the different analysis methods.

It is considered that the results for $m = 3$ are the closest to the true values of h, as the quality of fit shown in Table 1 suggests. However, Fig. 6 shows that the results for $m = 2$ are very close to those for $m = 3$, indicating that there would be no great advantage in proceeding to $m = 4$.

The differences in the values of h shown in Fig. 6 for $m = 0$, 1 and $1'$ can be explained by reference to Figs. 1 and 4. Fig. 1 shows that, for a given value Θ, an underestimate of τ (and hence of β_τ) will produce an underestimate of β (and hence of h); conversely, for a given value of β_τ, an overestimate of Θ will produce an

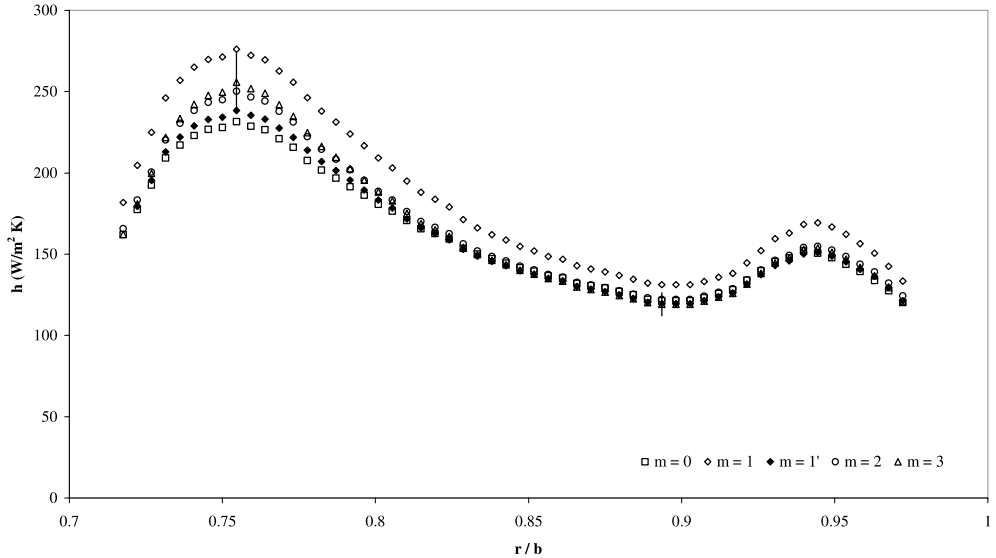

Fig. 6. Radial variation of h for different values of m (40 °C TLC) including uncertainty limits for $m = 3$.

overestimate of h. The $m = 0$ case corresponds to $\beta_\tau = 0$ in Fig. 1, and this leads to the underestimate of h shown in Fig. 6. Similarly, as can be seen in Fig. 4, the $m = 1'$ case underestimates τ and consequently underestimates h. For $m = 1$, the underestimate of $T_{aw,\infty}$ (which results from the underestimate of $T_{a,\infty}$ shown in Fig. 4 and Table 1) causes an overestimate of Θ, which in turn produces an overestimate of h. Fig. 6 shows that, for $m = 1$, h is overestimated everywhere, which means that the overestimate of Θ has a stronger effect than the underestimate of τ for this case.

From these results it is clear that neither the step-change nor the single-exponential provides the correct values of h for the experimental data considered here. Before drawing conclusions about the accuracy of the solutions for $m = 3$, it is appropriate to consider the experimental uncertainties in these solutions.

The uncertainty analysis given in 2 was used to create the "error bars" shown in Fig. 6. For the experimental measurements, $P_T \approx 0.3$ °C and $0.3 < \Theta < 0.75$, which results in $5.3 < \Phi_h^* < 6.3$. Consequently, $0.06 < P_h/h < 0.07$, and the maximum and minimum uncertainty limits, for the maximum and minimum values of h for $m = 3$, are shown in Fig. 6.

It should be pointed out that the median filtering of the TLC measurements and the smoothing of the air temperature measurements, described in Section 4, have created smoothed values of h, and the uncertainty limits shown in Fig. 6 are probably conservative. That the results for $m = 1'$ lie inside the uncertainty limits for $m = 3$ is fortuitous: for the reasons given above, the results for the step-change and single-exponential solutions are flawed and should be treated with suspicion.

Whilst the results discussed here have been produced from one test on one particular experimental set-up, it is considered that the exponential-series technique could be used successfully in those transient experiments in which it is not possible to achieve a satisfactory step-change in air temperature at the test section.

6. Conclusions

A new technique has been developed to determine values of the heat transfer coefficient, h, for "slow transient" experiments, in which it is not possible to achieve a step-change in the air temperature at the test section. The technique involves representing the measured temperature rise of the air by an exponential series and using this series as a boundary condition for Fourier's one-dimensional conduction equation. As for the step-change case, which is the limit of the exponential-series solution, it is not necessary to know the wall-temperature history: only a single narrow-band TLC is needed to determine h.

The technique has been demonstrated on measurements obtained in a test rig used to model the flow and heat transfer inside the pre-swirl cooling-air system of a gas-turbine engine. A mesh heater was used to generate a step-change in air temperature upstream of the test section; this produced a slow transient inside the test section itself. The air temperature history in the test section was represented by a series of m exponential terms, where $m = 0$, 1, 2 and 3 ($m = 0$ corresponding to the step-change case). Quality of fit criteria showed that the $m = 3$ curves provided the best fit, and the values of h obtained for this case were considered to be the most accurate. The results for $m = 2$ were very close to those for $m = 3$, but the values of h for $m = 0$ and 1 showed significant errors.

The new techniques should be applicable to many other slow transient heat transfer experiments.

References

Baughn, J.W., 1995. Liquid crystal methods for studying turbulent heat transfer. Int. J. Heat Fluid Flow 16, 365–375.

Butler, R.J., Baughn, J.W., 1996. The effect of the thermal boundary condition on transient method heat transfer measurements on a flat plate with a laminar boundary layer. J. Heat Transfer 118, 831–837.

Camci, C., Kim, K., Hippensteele, S.A., 1991. A new hue-capturing technique for the quantitative interpretation of liquid crystal images used in convective heat transfer studies. ASME Paper No. 91-GT-122.

Gillespie, D.R.H., Wang, Z., Ireland, P.T., 2001, Heater element. European patent No. 0847679.

Gillespie, D.R.H., Wang, Z., Ireland, P.T., 1998. Full surface local heat transfer coefficient measurements in a model of an integrally cast impingement cooling geometry. J. Turbomach. 120, 92–99.

Ireland, P.T., Jones, T.V., 2000. Liquid crystal measurements of heat transfer and surface shear stress. Meas. Sci. Technol. 11, 969–986.

Jones, T.V., Hippensteele, S.A., 1988. High-resolution heat-transfer-coefficient maps applicable to compound-curve surfaces using liquid crystals in a transient wind tunnel. NASA Technical Memorandum 89855.

Kasagi, N., Moffat, R.J., Hirata, M., 1989. Liquid crystals. In: Yang, W.J. (Ed.), Handbook of Flow Visualisation. Hemisphere, New York.

Karabay, H., Wilson, M., Owen, J.M., 2001. Predictions of effect of swirl on flow and heat transfer in a rotating cavity. Int. J. Heat Fluid Flow 22, 143–155.

Owen, J.M., Newton, P.J., Lock, G.D., 2003. Transient heat transfer measurements using thermochromic liquid crystal. Part 2: Experimental uncertainties. Int. J. Heat Fluid Flow 24, 23–28.

Pilbrow, R., Karabay, H., Wilson, M., Owen, J.M., 1999. Heat transfer in a "cover-plate" pre-swirl rotating-disc system. J. Turbomach. 121, 249–256.

Schultz, D.L., Jones, T.V., 1973. Heat transfer measurements in short duration hypersonic facilities. Agardograph 165.

Yan, Y., Gord, M.F., Lock, G.D., Wilson. M., Owen, J.M., 2002. Fluid dynamics of a pre-swirl rotating-disc system. ASME Paper No. GT-2002-30415, Trans. ASME, to be published.

Yan, Y., Owen, J.M., 2002. Uncertainties in transient heat transfer measurements with liquid crystal. Int. J. Heat Fluid Flow 23, 29–35.